Ultrashort-Pulse High-Power Yb^{3+}-Doped Fiber Amplifiers

Eldad Yahel, Ortwin Hess, and Amos A. Hardy, *Fellow, IEEE*

***Abstract*—Ultrashort optical pulse propagation in high-power Yb^{3+}-doped fiber amplifiers (YDFA) is studied using a spectrally resolved nonlinear power equation for the coupled pulse components. The Yb^{3+} ions transitions are modeled using a rate equation. Examples for high-power YDFAs with normal dispersion show good qualitative agreement with experimental results. We analyze the effects of the incident pulse wavelength, pulse peak power, Yb^{3+} concentration, pump filling factor, fiber length, pumping configuration, pump power and nonlinear index, on the intensity distribution of short amplified pulses. We also demonstrate the spectral compression of an initially negative-chirped pulse.**

***Index Terms*—Optical fiber amplifiers, optical fiber dispersion, optical fiber theory, optical pulse amplifiers, ytterbium (Yb).**

I. Introduction

HIGH-POWER short optical pulse amplification using cladding-pumped rare-earth doped fibers draws a great deal of interest for a variety of applications, e.g., in telecommunications, spectroscopy, materials processing and nonlinear frequency conversion [1]. Much attention has been paid to pulse amplification using normal dispersion doped fibers, where high-power parabolic pulses with a linear positive chirp across their central region can be produced. Such pulses propagate self-similarly with reduced distortions, and are efficiently recompressed into shorter duration using an anomalous dispersion medium [2]. Furthermore, initially negative-chirped pulses can be spectrally compressed in high-power doped fibers, to produce nearly transform-limited amplified pulses [3]. To these ends, Yb^{3+}-doped fiber amplifiers (YDFA), operating at a spectral range around 1.06 μm, are particularly attractive. YDFAs provide very broad gain bandwidth, high conversion efficiencies, and are relatively free of excited-state absorption and concentration quenching by ion-ion interactions [4].

Most theoretical works that discuss pulse amplification in YDFAs are based on the generalized nonlinear Schroedinger equation (NLSE) for the complex envelope of the amplified pulse [5]–[8]. Our goal in this contribution is twofold. First, we demonstrate the advantages of the simultaneous analysis of the spectral and temporal dependency of a propagating pulse in high-power, cladding-pumped YDFAs [9]. We recently used this approach to analyze relatively broad-bandwidth incident pulses in single-clad doped fibers, taking into account spatially and spectrally resolved gain and dispersion contributions, fiber nonlinearity, and amplified spontaneous emission (ASE) noise [10], [11]. Second, we extend previous works on pulsed YDFAs and describe numerical calculations using parameters that were not considered in detail before, such as the pulse wavelength, pulse peak power, Yb^{3+} concentration, pump filling factor, fiber length, pumping configuration and pump power.

This contribution is organized as follows. In Section II, we present the set of coupled rate-propagation equations for high-power pulsed YDFAs. In Section III, we show some numerical examples for ultrashort pulse amplification in high-power YDFAs, and consider the effect of various important design parameters on the amplified pulse shape. We also demonstrate spectral compression of an incident negative-chirped pulse. Our conclusions are discussed in Section IV. In Appendix A, we discuss the main assumptions leading to a spectrally resolved pulse propagation equation, whereas in Appendix B, we provide the finite difference scheme we used to solve the rate-propagation equations.

II. Theoretical Model

We consider a double-clad fiber geometry of length L, where the fiber core is uniformly doped with Yb^{3+} ions of concentration N_{Yb}. The pump power $P_p^{\pm}(z)$ at wavelength $\lambda = \lambda_p$ is coupled into the area of the first cladding (which includes the core), at either fiber ends. Thus, the pump propagates along the forward (positive) or the backward (negative) z directions, with an effective power filling factor Γ_p. Pump photons are absorbed by the Yb^{3+} ions in the ground $^2F_{7/2}$ state, exciting them to the $^2F_{5/2}$ state [4]. The ASE power densities $P^{\pm}(z,\lambda)$ that are emitted and amplified due to the Yb^{3+} ions transitions, propagate in both the positive and negative z direction. We assume that due to specialized fiber bending techniques, the amplification of high order modes in the core is practically suppressed. In that case, the wavelength-dependent power filling factor $\Gamma(\lambda)$ is approximated by the ratio of the LP_{01} modal power that is amplified in the core, to the total modal power [12].

The pulse spectral power density per unit wavelength $P_s(z,t,\lambda)$, is injected into the fiber at $z = 0$, and propagates in the forward z direction. We assume that the pulse power is strong enough to modify the population distribution of both the Yb^{3+} ions and host glass molecules. The power carried by the pump and ASE is much weaker than the pulse power, thus we restrict its effect to the Yb^{3+} transitions. We further assume that the atomic population within each Yb^{3+} energy manifold is in thermal equilibrium, and thus the gain-induced refractive index changes can be approximated using the Kramers–Kronig

Manuscript received January 29, 2007; revised April 26, 2007.

E. Yahel and O. Hess are with the Advanced Technology Institute, School of Electronics and Physical Sciences, University of Surrey, Guildford GU2 7XH, U.K. (e-mail: E.Yahel@surrey.ac.uk; O.Hess@surrey.ac.uk).

A. A. Hardy is with the Department of Electrical Engineering-Physical Electronics, Tel Aviv University, Tel Aviv 69978, Israel (e-mail: hardy@eng.tau.ac.il).

Digital Object Identifier 10.1109/JQE.2007.902390

transform of the gain coefficient [13]–[15]. We note that in practice the thermalization rate within each manifold depends to a large extent on the properties of the glass host, as well as on other conditions such as the temperature [14]. Thus, the extent to which the Yb^{3+} population deviates from thermal equilibrium during the pulse propagation requires further experimental validation. To be on the safe side, however, we consider here pulses with duration $\gtrsim$200 fs [14]. We also neglect the nearly wavelength-independent small index contribution from ultraviolet absorption to higher-order energy levels [16]. Under these assumptions, the bulk refractive index n_f that includes both linear and nonlinear contributions is given by

$$n_f(\rho,z,t,\lambda)=n(\rho,\lambda)+\delta n(\rho,z,t,\lambda) \tag{1}$$

where n is the (linear) refractive index of the passive fiber, and the nonlinear contribution δn is given by [13], [17]

$$\delta n(\rho,z,t,\lambda)\simeq\frac{\lambda}{4\pi}[N_2(\rho,z,t)(\bar{\sigma}_{21}(\lambda)+\bar{\sigma}_{12}(\lambda))-N_{\rm Yb}\bar{\sigma}_{12}(\lambda)] +n_2\int|U(\rho,\lambda')|^2\,P_s(z,t,\lambda')d\lambda'. \tag{2}$$

Here, n_2 is the nonlinear index, and $U(\rho,\lambda)$ is the envelope of the fundamental LP_{01} mode in the radial ρ direction along the fiber cross-section. We assume that $U(\rho,\lambda)$ is weakly dependent on the wavelength within the spectral band of the pulse, and that it is normalized to satisfy $2\pi\int|U(\rho,\lambda)|^2\rho d\rho=1$. The function $\bar{\sigma}_{ij}(\lambda)$ denotes the Kramers–Kronig transform of the cross section $\sigma_{ij}(\lambda)$ between levels i and j, and $N_2(\rho,z,t)$ is the atomic population of the excited $^2F_{5/2}$ manifold. We note that the index changes in (2) are assumed to be small, so that their effect on the modal envelope $U(\rho,\lambda)$ can be neglected. The nonlinear contribution to the refractive index δn induces dispersion and chirping of the propagating pulse. Further, the pulse is amplified, absorbed, and scattered along the optical fiber, due to the Yb^{3+} transitions and Rayleigh scattering. These effects can be included in a unified manner in a spectrally resolved propagation equation for the pulse power density, i.e., by considering the rate of change in the number of photons along the fiber, and the photons equation of motion [18]–[20]. Here, we assume that spatial perturbations in the refractive index along the propagation direction are small. We also assume that the pulse is short enough to justify neglecting the effect of transients in the pump power and ASE spectral densities powers on the Yb^{3+} population during the pulse propagation. Under these assumptions, we obtain the following set of propagation equations for the pulse spectral power density $P_s(z,t,\lambda)$, ASE spectral power density $P^{\pm}(z,\lambda)$, and the pump power $P_p^{\pm}(z)$, respectively (see Appendix A)

$$\frac{dP_s}{dz}+\frac{P_s}{c}\left(\frac{\partial\delta n_{\rm eff}^D}{\partial t}+\gamma\int\frac{\partial P_s}{\partial t}d\lambda\right) =g_{\rm eff}(z,t,\lambda)P_s+n_m\Gamma(\lambda)P_0(\lambda)\sigma_{21}(\lambda)N_2(z,t) \tag{3}$$

$$\pm\frac{dP^{\pm}}{dz}=g_{\rm eff}^0(z,\lambda)P^{\pm}+n_m\Gamma(\lambda)P_0(\lambda)\sigma_{21}(\lambda)N_2^0(z) \tag{4}$$

$$\pm\frac{dP_p^{\pm}}{dz}=\left[\Gamma_p\left[N_2^0(z)\left(\sigma_{21}(\lambda_p)+\sigma_{12}(\lambda_p)\right) -N_{\rm Yb}\sigma_{12}(\lambda_p)\right]-\alpha(\lambda_p)\right]P_p^{\pm}. \tag{5}$$

In (3), $dP_s/dz\equiv\partial P_s/\partial z+(V_{\rm eff}^{-1}+1/c\cdot[\gamma-\lambda\cdot d\gamma/d\lambda]\int P_s\cdot d\lambda)\cdot\partial P_s/\partial t+\lambda/c\cdot(\partial\delta n_{\rm eff}^D/\partial t+\gamma\int\partial P_s/\partial t\cdot d\lambda)\cdot\partial P_s/\partial\lambda$ and c is the speed of light in vacuum. The effective refractive index $n_{\rm eff}(z,t,\lambda)$ of the fundamental LP_{01} mode in the core is the sum of the linear passive contribution $n_{\rm eff}^L(\lambda)=2\pi\int n(\rho,\lambda)|U(\rho,\lambda)|^2\rho d\rho$ and the nonlinear gain-induced contribution $\delta n_{\rm eff}^D(z,t,\lambda)=\Gamma(\lambda)\cdot\lambda\cdot(4\pi)^{-1}\cdot[N_2(z,t)(\bar{\sigma}_{21}(\lambda)+\bar{\sigma}_{12}(\lambda))-N_{\rm Yb}\bar{\sigma}_{12}(\lambda)]$. The function $V_{\rm eff}(z,t,\lambda)\equiv[-\lambda^2/c\cdot\partial(n_{\rm eff}/\lambda)/\partial\lambda]^{-1}$ is the corresponding effective group velocity of the pulse spectral component at wavelength λ. The term $g_{\rm eff}(z,t,\lambda)=\Gamma(\lambda)[N_2(z,t)(\sigma_{21}(\lambda)+\sigma_{12}(\lambda))-N_{\rm Yb}\sigma_{12}(\lambda)]-\alpha(\lambda)$ is the effective local gain, where $\alpha(\lambda)$ represents an effective loss term due to scattering and fiber coiling. Other terms in (3)–(5) are the nonlinearity coefficient $\gamma(\lambda)=n_2/A_{\rm eff}$, where $A_{\rm eff}(\lambda)$ is an effective core area [21], and the functions $N_2^0(z)$ and $g_{\rm eff}^0(z,\lambda)$ that represent the steady state distributions of the excited $^2F_{5/2}$ state population and the effective local gain, respectively. The term $P_0(\lambda)=2hc^2/\lambda^3$ denotes the contribution of spontaneous emission into a mode, where the factor of two takes into account the possible orthogonal polarization directions [22]. Here we assume that spontaneous emission is generated into all n_m modes supported by the fiber [23]. It is worth mentioning the difference in the interpretation of the pulse energy distribution as derived from (3), i.e., $P_s(z,t,\lambda)$, and the pulse complex envelope as calculated from the solution of the generalized NLSE [21]. In particular, the pulse power, i.e., $\int P_s(z,t,\lambda)d\lambda$, and the pulse spectrum, i.e., $\int P_s(z,t,\lambda)dt$, that we calculate, represent the projections of many spectrally dependent temporal envelopes of the pulse energy components, and they are not derived from a Fourier transform. Furthermore, it is clear that our approach cannot describe some of the wave properties of the pulse, e.g., as manifested in the contribution of different phases to a nonlinearity-generated pulse spectral component [21], [24]. However, frequency mixing of the pulse spectral components is properly considered in our formalism.

The quasi-three-level Yb^{3+} system is assumed to have two energy manifolds [4]. Hence, the excited $^2F_{5/2}$ population, N_2, satisfies the following rate equation:

$$\frac{\partial}{\partial t}N_2(z,t)=-N_2(z,t)\left[\frac{1}{\tau_{\rm Yb}}+W_{12}(z,t)+W_{21}(z,t)\right] +W_{12}(z,t)N_{\rm Yb} \tag{6}$$

where $\tau_{\rm Yb}$ is the lifetime of the Yb^{3+} excited $^2F_{5/2}$ state. The terms W_{12} and W_{21} in (6) represent stimulated absorption and emission rates, respectively, and depend on the pump power, pulse power, and ASE power emitted by the Yb^{3+} ions. These terms are given by

$$W_{ij}(z,t)=\frac{\Gamma_p\sigma_{ij}(\lambda_p)\left[P_p^+ + P_p^-\right]\lambda_p}{hcA_{\rm core}} +\frac{1}{hcA_{\rm core}}\int\Gamma(\lambda)\sigma_{ij}(\lambda)P_s\lambda d\lambda +\frac{1}{hcA_{\rm core}}\int\Gamma(\lambda)\sigma_{ij}(\lambda)[P^+ + P^-]\lambda d\lambda \tag{7}$$

where $A_{\rm core}$ is the area of the fiber core. Here, the limits of the first and the second integrals on the RHS of (7) are determined

by the spectral bandwidth of the pulse and the cross section of the ${}^2F_{7/2} - {}^2F_{5/2}$ transitions of Yb^{3+} ions, respectively.

In order to solve (3)–(6) numerically, we divide the ASE spectrum in the wavelength range from 850 to 1140 nm into channels of width $\Delta\lambda = 1$ nm. Furthermore, the pulse bandwidth around the central wavelength λ_s is divided into channels of width $\Delta\lambda_s \simeq 0.2$ nm. Equations (3)–(6) are initially solved assuming steady state conditions without pulse injection [i.e., $\partial/\partial t \equiv 0$ and $P_s(z=0,\lambda)=0$]. To this end, we integrate the equations iteratively along the forward and backward propagation direction, until the overall power channels converge. For the time dependent pulse propagation, we use a finite difference scheme with two staggered grids for the photons and the ions populations. The numerical solution of (3) is considerably simplified by transforming the equation into a retarded time frame moving with a constant reference group velocity V_g^R. Thus, we define a reduced time $T \equiv t - z/V_g^R$, so that (3) becomes

$$\frac{\partial P_s}{\partial z} + \left(\left[V_{\text{eff}}^{-1} - \left(V_g^R\right)^{-1}\right] + \frac{1}{c}\left[\gamma - \lambda\frac{d\gamma}{d\lambda}\right]\int P_s d\lambda\right)\frac{\partial P_s}{\partial T} + \frac{1}{c}\left(\frac{\partial \delta n_{\text{eff}}^D}{\partial T} + \gamma\int\frac{\partial P_s}{\partial T}d\lambda\right)\left(P_s + \lambda\frac{\partial P_s}{\partial \lambda}\right) = g_{\text{eff}}(z,T,\lambda)P_s + n_m\Gamma(\lambda)P_0(\lambda)\sigma_{21}(\lambda)N_2(z,T). \quad (8)$$

Equations (8) and (6) are solved numerically using an implicit upwind finite-difference scheme, with an iterative algorithm to solve the coupled pulse spectral components at each spatial and temporal step (cf. Appendix B) [25]. We note that the numerical stability of this scheme depends on the pulse power at the boundaries of the spectral window, which has to be sufficiently small in order to ensure that the effects of numerical reflections from these boundaries are negligible. To this end, we employed a large enough spectral window with strongly absorbing spectral boundaries.

III. Examples

In order to analyze high-power pulse amplification in YDFAs, we consider several examples near the 1060-nm transition. Unless otherwise mentioned, the parameters assumed in the numerical calculations correspond to the experimental YDFA described in [1], [5] and are summarized in Table I. The effective linear index contribution $n_{\text{eff}}^L(\lambda)$ is calculated based on the waveguide dispersion relations [12], taking into account Sellmeier's equation for silica host [21]. We also assume that the pump power ($P_p \simeq 5$ W) is injected at $z = L$, i.e., counter-propagating to the incident pulse, and that it provides approximately 32-dB gain at $\sim$1060 nm. Based on these assumptions, we calculated the spectrum of the fiber dispersion parameter, i.e., $D = -\lambda/(Lc)\cdot d^2[\int_0^L n_{\text{eff}}dz]/d\lambda^2$ (cf. Fig. 1). We note that due to the strong gain-induced contribution, the fiber dispersion fluctuates strongly at a spectral range near $\lambda \simeq 976$ nm, where the fiber becomes strongly absorbing. In the spectral range relevant to optical amplification, i.e., at $1015 \lesssim \lambda \lesssim 1120$ nm (see inset), the dispersion is normal, and it monotonically increases from $D \simeq -40$ to $D \simeq -20$ ps $\cdot$ km^{-1} $\cdot$ nm^{-1}. Thus, gain-induced dispersion fluctuations are expected to have only small effect on an amplified pulse, in contrast to Er^{3+}-doped fibers [10].

TABLE I
Parameters Used in the Numerical Calculations

Parameter	Value	Notes
λ_s	1060 nm	
λ_p	976 nm	
τ_{Yb}	1 msec	
$\sigma_{12}(\lambda)$, $\sigma_{21}(\lambda)$		Ref. [4]
A_{core}	7.1×10^{-10} m^2	Ref. [5]
n_2	3.5×10^{-20} m^2 W^{-1}	Based on Ref. [5]
NA	0.06	Ref. [5]
n_m	4	Ref. [5]
α	5×10^{-3} m^{-1}	
$n_{\text{eff}}^L(\lambda)$		Based on Ref. [12], [21]
$\Gamma(\lambda)$		Ref. [12]
Γ_p	6×10^{-3}	
L	9 m	Ref. [5]
N_{Yb}	2.2×10^{25} m^{-3}	Ref. [5]

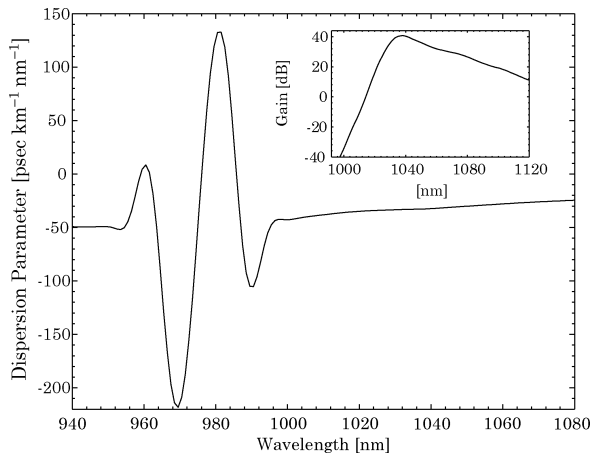

Fig. 1. Dependence of the fiber dispersion parameter (D) on the wavelength. The inset shows the spectrum of the integrated fiber gain, i.e., $G(0,L,\lambda) \equiv \exp[\int_0^L g_{\text{eff}}dz]$.

In what follows, we demonstrate the effects of various physical parameters on the spectral and temporal characteristics of a short amplified pulse. In particular, we study within the framework of our model the effects of the incident pulse wavelength, pulse peak power, Yb^{3+} concentration, pump filling factor, fiber length, pumping configuration, pump power and the nonlinear index. Unless stated otherwise, we assume throughout this paper that the incident pulse spectral power density distribution, i.e., $P_s(z=0,t,\lambda)$, is given by the Wigner function of a chirp-free Gaussian pulse centered at $t = 0$, with width [full-width at half-maximum (FWHM)] of $T_0 \simeq 270$ fs, and peak power of

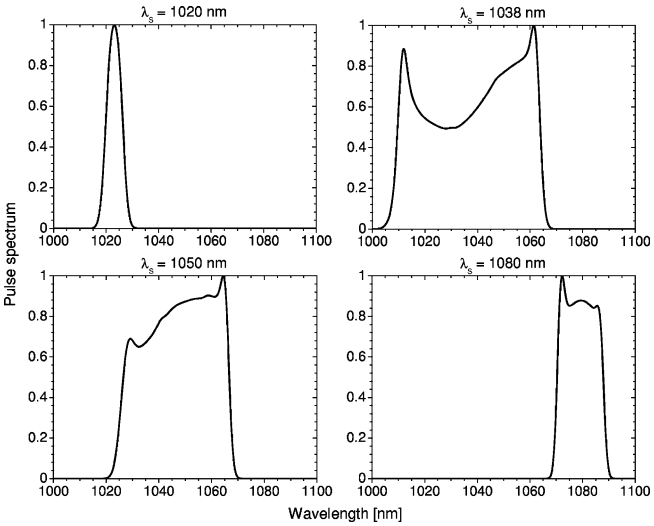

Fig. 2. Amplified pulse energy spectrum, i.e., $\int P_s(z = L, t, \lambda)dt$ (normalized), as function of the wavelength, for incident pulses with different central wavelengths λ_s in the range 1020–1080 nm.

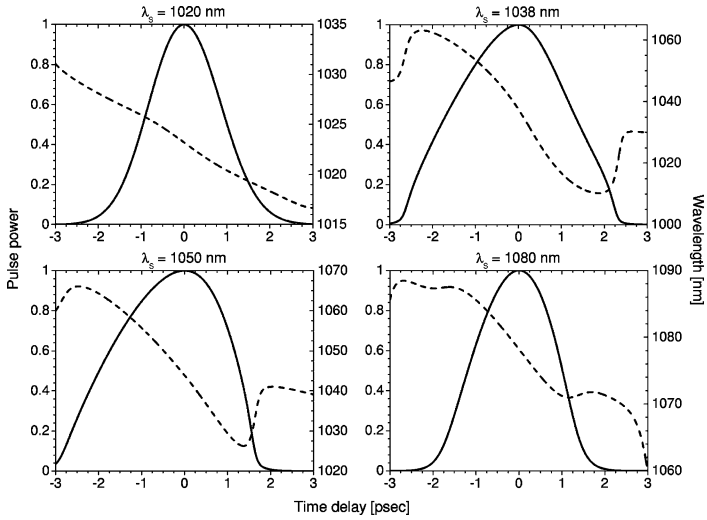

Fig. 3. Amplified pulse power, i.e., $\int P_s(z = L, t, \lambda)d\lambda$ (solid line, normalized), and the amplified pulse mean wavelength (dashed line), as function of the time delay in respect to the arrival time of the pulse peak, for incident pulses with different central wavelengths λ_s in the range 1020–1080 nm.

$\sim$214 W [26]. Thus, the incident pulse is transform-limited, with a bandwidth of $\sim$6 nm.

In Fig. 2 we depict the dependence of the amplified pulse spectrum on the wavelength, for different incident pulse central wavelengths λ_s. We note that on shifting the incident pulse wavelength from λ_s =1020 to 1080 nm, the amplified pulse spectrum changes its shape due to the nonuniformity of the gain (cf. Fig. 1). The spectral broadening of the amplified pulse is a consequence of the nonlinearity-induced chirp, which in turn depends on the pulse power through (2). Thus, spectral broadening is most significant for a pulse incident near the gain peak wavelength, e.g., at $\lambda_s \simeq 1038$ nm. It is worth to mention, however, that the amplified spectrum of a weak pulse is predominantly affected by gain narrowing [10]. We note that the pulse gain is relatively small in the short tail of the gain spectrum, e.g., for $\lambda_s \simeq 1020$ nm, and hence spectral broadening is also small. Our results also show that in the moderate gain regime, e.g., for the case $\lambda_s \simeq 1080$ nm, the amplified spectrum is relatively flat shaped with steep edges. The corresponding dependence of the amplified pulse power on the delay time with respect to the arrival of the pulse peak is depicted in Fig. 3. Here we also show the amplified pulse mean wavelength, i.e., $\int \lambda P_s(z = L, t, \lambda)d\lambda / \int P_s(z = L, t, \lambda)d\lambda$ [26], as function of the time delay. We note that the amplified pulse broadens in time due to propagation in the normal dispersion regime, and that the wavelength chirp is positive during the arrival time of the main part of the amplified pulse (i.e., the mean pulse frequency increases during that time). The wavelength chirp is approximately linear across the $\lambda_s \simeq 1080$ nm pulse, where the amplified pulse shape is nearly parabolic. On the other hand, the wavelength chirp deviates from linearity close to the gain-peak wavelength (e.g., for $\lambda_s \simeq 1050$ nm). Thus, we conclude that a deviation of the amplified pulse spectrum from flatness (cf. Fig. 2) corresponds to a nonlinear pulse chirp [6].

Fig. 4 shows the spectrum and power of an amplified pulse for different incident pulse peak powers. The intensity of the amplified pulse in the limit of weak and moderate peak powers,

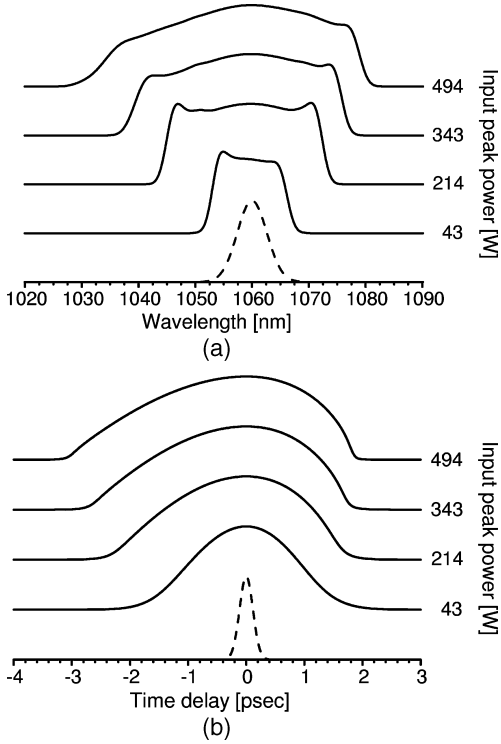

Fig. 4. Amplified pulse intensity distribution for different incident pulse peak powers. The solid and dashed lines correspond to the normalized intensity distribution of the pulse at $z = L$ and $z = 0$, respectively. (a) Pulse spectrum. (b) Pulse power.

e.g., $\lesssim$210 W, corresponds to the parabolic pulse regime. On increasing the peak power, e.g., $\gtrsim$340 W, the effect of fiber nonlinearity is enhanced and the amplified pulse spectrum broadens significantly, in agreement with experimental measurements under similar conditions [1], [5]. In particular, we note that the asymmetries in the pulse spectra are consequence of the inclusion of a realistic gain term in (3), whereas theoretical models that are based on a more simplified approach to the

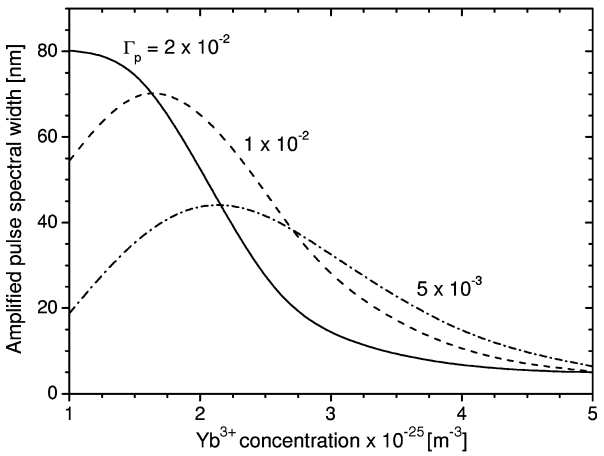

Fig. 5. Dependence of the amplified pulse spectral width, on the Yb^{3+} concentration (N_{Yb}), for a pulse incident around $\lambda_s = 1038$ nm, and for different values of the effective pump filling factor (Γ_p). The lines represent a B-spline interpolation of the exact numerical solution.

dopant transitions predict a perfectly symmetric spectrum, e.g., see [5]. On further increasing the peak power, e.g., $\simeq$490 W, the amplified spectrum is strongly reshaped due to the finite gain bandwidth [Fig. 4(a)]. In this regime, the amplified pulse power deviates asymmetrically from a parabolic shape, and is characterized by the much longer leading edge [Fig. 4(b)]. This reshaping is a consequence of an increase in the group index at the pulse peak power, which enhances the generation of blue-shifted spectral components.

Next, we consider the effect of the Yb^{3+} concentration on the amplified pulse characteristics. Fig. 5 shows the amplified pulse spectral width, as function of the Yb^{3+} concentration, for different values of the effective pump filling factor. Depending on the Yb^{3+} concentration, the spectral width of the amplified pulse is maximized where the gain is also maximized. Further increasing the Yb^{3+} concentration results in a decrease of the amplified pulse power due to absorption losses, and hence to reduced spectral broadening of the amplified pulse. Our results demonstrate that in the limit of small Yb^{3+} concentrations, increasing the pump filling factor (e.g., by coiling the fiber to enhance pump absorption efficiency [27]) broadens the spectral width of the output pulse. We also find that there is a positive correlation between the dependency of the pulse temporal width on the Yb^{3+} concentration and the corresponding dependency of the spectral width, as the former depends on the differences in the group velocities of the pulse spectral components. These differences, in turn, tend to increase with the spectral redistribution of the pulse energy due to the nonlinearity-induced chirp.

Fig. 6 shows the amplified pulse power and pulse spectrum as function of the fiber length (for $\Gamma_p = 0.02$). We note that on increasing the fiber length, the amplified pulse temporal width continuously increases due to the dispersion of the pulse spectral components. There is an optimum fiber length, for a given pump power, at which the amplified pulse peak power is maximized, e.g., at $L = 6$ m [Fig. 6(a)]. This peak power, in turn, also maximizes nonlinear effects. Thus, the amplified pulse spectrum broadens as long as the fiber length is shorter than this optimum length, and it narrows for longer lengths while the pulse energy

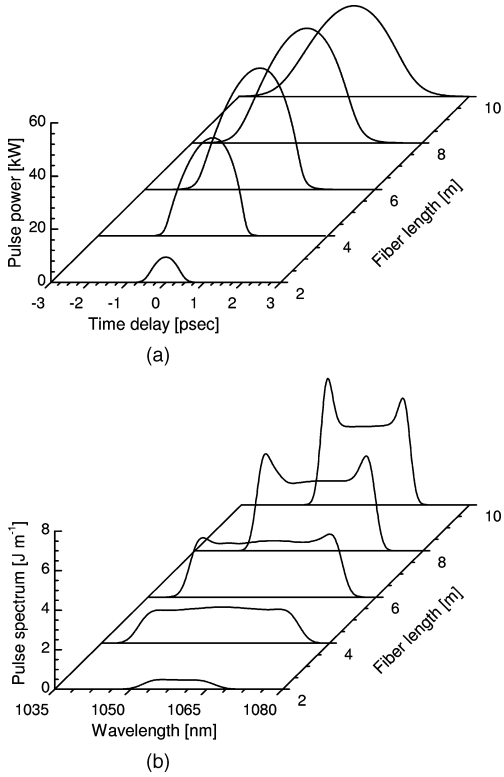

Fig. 6. Dependence of the amplified pulse intensity on the fiber length (L), as function of (a) the time delay and (b) the wavelength.

is redistributed towards the edges of the spectrum [Fig. 6(b)]. We also find that the amplified pulse characteristics depend on the pumping configuration. For example, the amplified pulse spectral and temporal widths are somewhat larger in a copropagating configuration, in particular in the limit of long fibers (e.g., $L \simeq 10$ m). We attribute this result to the spatial distribution of the population inversion in a copropagating configuration, which is maximized near $z = 0$. Thus, an incident pulse encounters relatively high gain, which, in turn, results in a bigger product of pulse power and propagation distance, and hence stronger nonlinear effects. It should be also noted that losses to stimulated Raman scattering (which are neglected in this work) ultimately limit the optimum fiber length below some critical length that depends on the incident pulse peak power and on the fiber gain [28].

An all important parameter in our model is the numerical value of the nonlinear index n_2. The value of this parameter depends on the properties of the glass host, and its measured value in silica glass varies significantly [21]. In order to examine the effect of n_2 on our results, we artificially changed its value between 2.2×10^{-20} to 3.9×10^{-20} $m^2 \cdot W^{-1}$ [21]. In Fig. 7 we depict the amplified pulse output energy as function of the injected pump power, for two values of n_2. We note that the output pulse energy saturates, more significantly for higher n_2 (i.e., $n_2 = 3.9 \times 10^{-20}$ $m^2 \cdot W^{-1}$). This saturation is a consequence of the finite gain bandwidth of the Yb^{3+} ions, which limits the bandwidth of the amplified pulse, and hence its output energy [5], [29]. The amplified pulse bandwidth, in turn, depends on the nonlinearity-induced chirp, and it increases with the pump power [30], and with the value of n_2 (see inset). The effect of n_2 on the amplified pulse is most significant at high pump

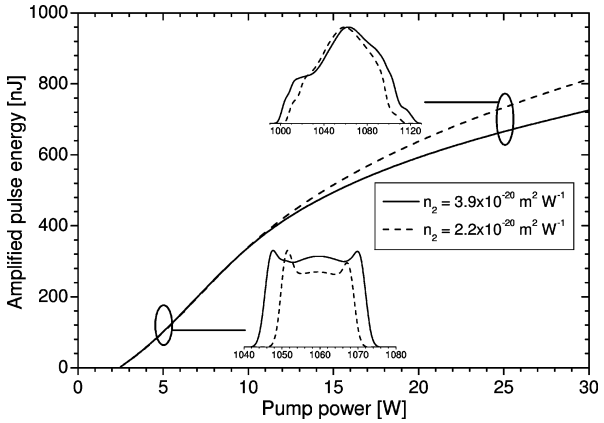

Fig. 7. Dependence of the amplified pulse energy on the injected pump power (P_p), for two different values of the nonlinear index (n_2). The lines represent a B-spline interpolation of the exact numerical solution. Inset: the pulse spectrum for pump powers of 5 and 25 W. The horizontal line (inset) is wavelength in nanometers.

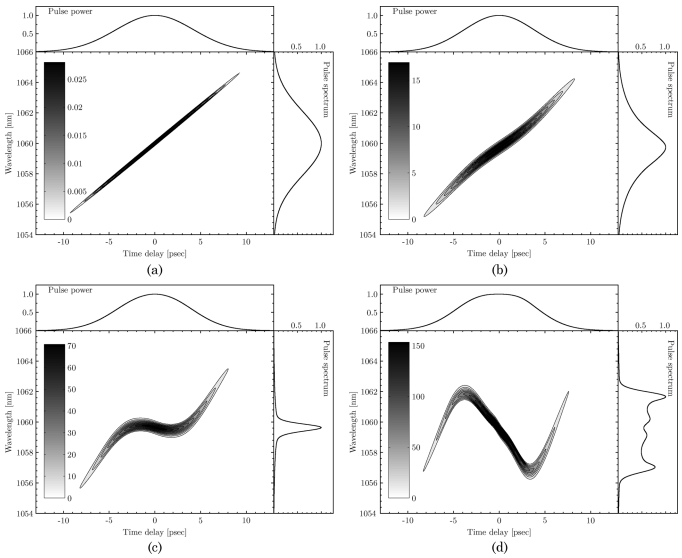

Fig. 8. Contour plot of the pulse spectral power density (in terawatts per unit wavelength, see the gray palette inset), as function of the wavelength and time delay. Top: pulse power (normalized). Right side: pulse spectrum (normalized). (a). Incident pulse at $z = 0$. (b)–(d) Correspond to the pulse spectral power density at $z = L$ for an injected pump power (P_p) of 5, 10, and 25 W, respectively.

powers, where the spectral bandwidth of the amplified pulse is comparable with the gain bandwidth. In that regime, the amplified pulse spectrum is severely deformed, its chirp strongly deviates from linearity, and the pulse recompression efficiency is degraded [5]. It is clear that the saturation exhibited here can be removed by reducing the peak power of the incident pulse (cf. Fig. 4), e.g., by using gratings to stretch the pulse before amplification [1].

Finally, we demonstrate the amplification of an initially chirped pulse. To this end, we assume that the incident Gaussian pulse is stretched to $T_0 = 10$ ps, and its peak power is correspondingly reduced to $\sim$6 W. This stretching, in turn, induced a pulse chirp, e.g., $\beta \simeq -30/T_0^2$ (see [26, eq. (5.15)]). Fig. 8(a) depicts the incident chirped pulse spectral power density distribution as function of the wavelength and time delay, whereas Fig. 8(b)–(d) shows the corresponding amplified pulse spectral power density, for different pump powers. For low pump powers, e.g., $P_p \simeq 5$ W, the gain and hence the nonlinearity-induced chirp are relatively small, having only moderate effect on the amplified pulse [Fig. 8(b)]. Further increasing the pump power, e.g., $P_p \simeq 10$ W, the induced positive chirp cancels the initial chirp over the pulse central region, producing significant spectral compression [see Fig. 8(c)]. This result is in qualitative agreement with experimental measurements [3], and it is the key for achieving transform-limited amplified pulses. On further increasing the pump power, e.g., $P_p \simeq 25$ W, the core of the amplified pulse becomes positively chirped, resulting in somewhat broadening of the output spectrum [Fig. 8(d)]. We note that for the calculated pulse parameters there is only a small decrease in the compression ratio of the output pulse duration with increasing pump power. We thus conclude that there is an optimum pump power for achieving an amplified pulse with the smallest time–bandwidth product.

IV. Conclusion

In this work, we analyzed ultrashort pulse amplification in high-power YDFAs using the numerical solution of a time-dependent, spectrally resolved pulse propagation equation. We demonstrated the dependence of the amplified pulse energy spectrum and pulse power on the pulse wavelength and peak power. It was shown that an efficient amplification of linear wavelength chirped parabolic pulses can be achieved with a limited incident pulse peak power and by tuning the incident pulse wavelength to the longer tail of the gain spectrum. On the other hand, the amplified pulse spectral width increases on increasing the incident pulse peak power or on tuning the incident pulse wavelength towards the gain-peak wavelength. This broadening, in turn, distorts the amplified pulse shape, and degrades the linear wavelength chirp. We also found that the spectral width of the amplified pulse can be controlled by properly choosing the Yb^{3+} concentration and the effective pump filling factor. In particular, for a given fiber properties, there exists an Yb^{3+} concentration value that maximizes the spectral bandwidth of the amplified pulse. This value tends to be smaller for more efficiently absorbing fibers. We calculated an optimum fiber length for which the amplified pulse peak power is maximized, its spectrum is relatively flattened, and its wavelength chirp is approximately linear. For fibers longer than this optimum, the pulse energy redistributes towards the spectral wings and the wavelength chirp deviates from linearity, while shorter fibers are less efficient. For sufficiently increased pump power, the amplified pulse energy saturates since its spectral bandwidth is limited by the finite gain bandwidth of Yb^{3+} ions. This saturation is only weakly dependent on the measured values of the nonlinear index of silica glass. We also demonstrated that by tuning the pump power, the amount of spectral compression of a negative-chirp incident pulse can be controlled. Our results provide additional support to experimental measurements of broad-bandwidth amplified pulses, which extends the standard NLSE formalism and can, in principle, be compared directly with the pulse spectrogram [10]. Furthermore, the model allows the inclusion of a realistic gain spectrum for the Stark-splitted doped ions transitions using measured cross sections, therefore alleviating some of the restrictions imposed by analytical gain

approximations [7]. With some minor modifications, the model presented herein can be also employed to other types of doped fibers, as well as to different incident pulse shapes.

APPENDIX A
SPECTRALLY RESOLVED PROPAGATION EQUATION

Photon transfer in a general dispersive, isotropic medium, whose properties can also change in time and space, was considered in detail in the framework of radiative transfer theory [19], [20]. Here we apply this theory to model pulse amplification along an YDFA. We define the distribution function $f(\underline{r},t,\nu)$ of photons that propagate in the forward z direction along the fiber such that $fd^3rd\nu$ is the number of photons at time t in differential volume element d^3r, in frequency interval $d\nu$, centered at $(\underline{r},\nu)$. The number of photons change in time as the photons stream along the fiber, due to the interaction of photons with the Yb^{3+} ions and the glass host molecules, e.g., due to stimulated emission, absorption, and scattering of photons. Thus, we have the following balance equation

$$\frac{d}{dt}(fd^3rd\nu) = g(\underline{r},t,\nu)V_g f(\underline{r},t,\nu)d^3rd\nu + n_m\sigma_{21}(\nu)N_2(\underline{r},t)V_g f_0(\underline{r},\nu)d^3rd\nu \quad \text{(A1)}$$

where $g(\underline{r},t,\nu) \equiv N_2(\underline{r},t)(\sigma_{21}(\nu)+\sigma_{12}(\nu)) - N_{\mathrm{Yb}}\sigma_{12}(\nu) - \alpha(\nu)$ is the local gain per unit length, which includes the dopant contribution and scattering losses $\alpha(\nu)$. The function $f_0(\underline{r},\nu)$ is the distribution of photons that contribute to spontaneous emission into one mode, n_m is the effective number of transverse fiber modes and $V_g(\underline{r},t,\nu)$ denotes the photons group velocity in the fiber. Following some algebraic manipulations, it is straightforward to obtain [20]

$$\frac{\partial f}{\partial t} + \nabla_{\underline{r}}\cdot\left(\frac{d\underline{r}}{dt}f\right) + \frac{\partial}{\partial\nu}\left(\frac{d\nu}{dt}f\right) = g(\underline{r},t,\nu)V_g f(\underline{r},t,\nu) + n_m\sigma_{21}(\nu)N_2(\underline{r},t)V_g f_0(\underline{r},\nu). \quad \text{(A2)}$$

Introducing the optical intensity per unit bandwidth $I_s(\underline{r},t,\nu)\equiv h\nu V_g f$, representing a time-frequency distribution of an amplified pulse along the fiber [9], and making use of the derivative along the propagation path, i.e., $d/dt = V_g\cdot d/dz$, allows us to write (A2) as

$$\frac{\partial}{\partial t}\left(\frac{I_s}{V_g}\right) + \frac{\partial I_s}{\partial z} + \nu\frac{\partial}{\partial\nu}\left(\frac{1}{\nu}\frac{d\nu}{dz}I_s\right) = g(\underline{r},t,\nu)I_s(\underline{r},t,\nu) + n_m\sigma_{21}(\nu)N_2(\underline{r},t)I_0(\underline{r},\nu) \quad \text{(A3)}$$

where $I_0(\underline{r},\nu)\equiv h\nu V_g f_0$ is the spontaneous emission intensity per unit bandwidth into one mode. We note that the photon equation of motion can be written as [19]

$$\frac{d\nu}{dz} = -\frac{\nu}{c}\frac{\partial n_f}{\partial t} \quad \text{(A4)}$$

where the bulk refractive index $n_f(\underline{r},t,\nu)$ is given explicitly by [13], [17]

$$n_f(\underline{r},t,\nu) = n(\underline{r},\nu) + \frac{c}{4\pi\nu}\left[N_2(\underline{r},t)\left(\bar{\sigma}_{21}(\nu)+\bar{\sigma}_{12}(\nu)\right) - N_{\mathrm{Yb}}\bar{\sigma}_{12}(\nu)\right] + n_2\int I_s(\underline{r},t,\nu)d\nu. \quad \text{(A5)}$$

Substituting (A4) into (A3) and making use of the explicit form of the group velocity, i.e., $V_g(\underline{r},t,\nu)\equiv[1/c\cdot\partial(\nu n_f)/\partial\nu]^{-1}$, we derive the following equation for the rate of change in the pulse intensity per unit bandwidth along the fiber

$$\frac{1}{c}\frac{\partial(\nu n_f)}{\partial\nu}\frac{\partial I_s}{\partial t} + \frac{\partial I_s}{\partial z} - \frac{\nu}{c}\frac{\partial n_f}{\partial t}\frac{\partial I_s}{\partial\nu} + \frac{I_s}{c}\frac{\partial n_f}{\partial t} = g(\underline{r},t,\nu)I_s(\underline{r},t,\nu) + n_m\sigma_{21}(\nu)N_2(\underline{r},t)I_0(\underline{r},\nu). \quad \text{(A6)}$$

We note that for an effectively single-mode pulse propagation, radiation modes can be ignored. Assuming that only the modal gain varies in the propagation direction, we define the power density per unit bandwidth, P_s, by

$$I_s(\underline{r},t,\nu) \simeq |U(\rho,\nu)|^2 P_s(z,t,\nu). \quad \text{(A7)}$$

We also assume

$$I_0(\underline{r},\nu) \simeq |U(\rho,\nu)|^2 P_0(\nu) \quad \text{(A8)}$$

where $P_0(\nu) = 2h\nu$ is the contribution of spontaneous emission into the mode [22]. Substituting (A5), (A7), and (A8) into (A6), and integrating over the entire transverse cross section, we obtain (3) in the text for the spectral power density. We note that this procedure essentially assumes that the effective index contributions in (3) can be calculated based on the variation theorem. Similarly, we derive steady-state expressions for the ASE spectral power densities and the pump power, given by (4) and (5), respectively, where we also assume forward and backward propagation.

APPENDIX B
FINITE-DIFFERENCE SCHEME

To solve (8), we assume equally spaced intervals along the z axis with spatial grid points $z_k = (k-1)\Delta z (k = 1,2,\ldots,k_{\max})$, equally spaced spectral intervals with wavelength grid points $\lambda_l = \lambda_{\min}(l-1)\Delta\lambda_s (l = 1,2,\ldots,l_{\max})$, and a temporal grid $T_n = (n-1)\Delta T (n = 1,2,\ldots,n_{\max})$. Here, $\lambda_{\min}$ is the lower limit wavelength of the spectral window. We employ different, staggered, grids for the photons and ions equations, i.e., (8) and (6), which are half time step $\Delta T/2$ and half spatial step $\Delta z/2$ shifted with respect to each-other. The forward upwind finite-difference approximation for (8), e.g., is as follows:

$$\left(\frac{\partial P_s}{\partial z}\right)^l_{n,k-\frac{1}{2}} + \left(I^l_{n,k} - \left(V_g^R\right)^{-1} + \frac{\Delta\lambda_s}{c}\left[(\gamma)^l - (\lambda)^l\left(\frac{d\gamma}{d\lambda}\right)^l\right] \times \sum_l (P_s)^l_{n-\frac{1}{2},k-\frac{1}{2}}\right)\left(\frac{\partial P_s}{\partial T}\right)^l_{n-\frac{1}{2},k} + \frac{1}{c}\left(H^l_{n,k} + (\gamma)^l\Delta\lambda_s\sum_l\left(\frac{\partial P_s}{\partial T}\right)^l_{n-\frac{1}{2},k}\right) \times \left[(P_s)^l_{n-\frac{1}{2},k-\frac{1}{2}} + (\lambda)^l\left(\frac{\partial P_s}{\partial\lambda}\right)^l_{n,k}\right] \simeq G^l_{n,k}(P_s)^l_{n-\frac{1}{2},k-\frac{1}{2}} + F^l_{n,k}, \quad \text{(B1)}$$

where the quantities $F^l_{n,k}$, $G^l_{n,k}$, $H^l_{n,k}$, and $I^l_{n,k}$ are related to the host dispersion and dopant contributions. These terms

are defined on the point (n,k,l) of the ions grid, and are given by

$$F^l_{n,k} \equiv n_m(\Gamma)^l(P_0)^l(\sigma_{21})^l(N_2)_{n,k} \tag{B2}$$

$$G^l_{n,k} \equiv (\Gamma)^l\left[(N_2)_{n,k}\left((\sigma_{21})^l+(\sigma_{12})^l\right) - N_{\mathrm{Yb}}(\sigma_{12})^l\right]-(\alpha)^l \tag{B3}$$

$$H^l_{n,k} \equiv \frac{(\Gamma)^l(\lambda)^l}{4\pi}\left(\frac{\partial N_2}{\partial T}\right)_{n,k}\left[(\bar{\sigma}_{21})^l+(\bar{\sigma}_{12})^l\right] \tag{B4}$$

$$I^l_{n,k} \equiv \frac{1}{c}\left[\left(n^L_{\mathrm{eff}}\right)^l+\left(\delta n^D_{\mathrm{eff}}\right)^l_{n,k}\right] - \frac{(\lambda)^l}{c}\left[\left(\frac{dn^L_{\mathrm{eff}}}{d\lambda}\right)^l+\left(\frac{\partial \delta n^D_{\mathrm{eff}}}{\partial\lambda}\right)^l_{n,k}\right]. \tag{B5}$$

In order to solve the nonlinear equation (B1), we assume that the terms $F^l_{n,k}$, $G^l_{n,k}$, $H^l_{n,k}$ and $I^l_{n,k}$ are all known for the row n of the ions grid. Furthermore, we assume that $(P_s)^l_{n-1,k}$ are known for all values of l and k, and that $(P_s)^l_{n,k-1}$ is also known on the photons grid. Under these assumptions, the numerical solution of (B1) on row n of the photons grid starts from the boundary at $k=1(z=0)$. At each integration step, we employ an iterative algorithm for the nonlinear terms, which can be written as [25]

$$\begin{aligned}&\left(\left[(P_s)^{l+1}_{n,k}\right]^{s+1}-\left[(P_s)^{l-1}_{n,k}\right]^{s+1}\right)\frac{(\lambda)^l}{2c\Delta\lambda_s}J^l_{n,k}\\ &+\frac{1}{4}\left[(P_s)^l_{n,k}\right]^{s+1}\left[\frac{4}{\Delta z}-G^l_{n,k}+\frac{J^l_{n,k}}{c}+\frac{4K^l_{n,k}}{\Delta T}\right]\\ &\simeq\frac{1}{\Delta z}(P_s)^l_{n,k-1}+F^l_{n,k}+\frac{K^l_{n,k}}{\Delta T}(P_s)^l_{n-1,k}+\frac{1}{4}\left[G^l_{n,k}-\frac{J^l_{n,k}}{c}\right]\\ &\times\left[(P_s)^l_{n-1,k-1}+(P_s)^l_{n-1,k}+(P_s)^l_{n,k-1}\right]\end{aligned} \tag{B6}$$

where

$$J^l_{n,k} \equiv H^l_{n,k}+\frac{(\gamma)^l\Delta\lambda_s}{\Delta T}\sum_l\left(\left[(P_s)^l_{n,k}\right]^s-(P_s)^l_{n-1,k}\right) \tag{B7}$$

$$\begin{aligned}K^l_{n,k} \equiv{}& I^l_{n,k}-\left(V^R_g\right)^{-1}+\frac{\Delta\lambda_s}{4c}\left[(\gamma)^l-(\lambda)^l\left(\frac{d\gamma}{d\lambda}\right)^l\right]\\ &\cdot\sum_l\Big(\left[(P_s)^l_{n,k}\right]^s+(P_s)^l_{n-1,k-1}\\ &+(P_s)^l_{n-1,k}+(P_s)^l_{n,k-1}\Big).\end{aligned} \tag{B8}$$

Here, the superscript s denotes the iteration number for solving the tridiagonal system of equations (B6), e.g., using the method of Gaussian elimination and back-substitution. For the initial iteration, i.e., $s=0$, we employ $\left[(P_s)^l_{n,k}\right]^0=(P_s)^l_{n-1,k}$. The iterations continue until convergence, at each integration step along the fiber.

REFERENCES

[1] J. Limpert, F. Roser, T. Schreiber, and A. Tunnermann, "High-power ultrafast fiber laser systems," *IEEE J. Sel. Top. Quantum Electron.*, vol. 12, no. 2, pp. 233–244, Mar. 2006.

[2] M. E. Fermann, V. I. Kruglov, B. C. Thomsen, J. M. Dudley, and J. D. Harvey, "Self-similar propagation and amplification of parabolic pulses in optical fibers," *Phys. Rev. Lett.*, vol. 84, no. 26, pp. 6010–6013, Jun. 2000.

[3] J. Limpert, T. Gabler, A. Liem, H. Zellmer, and A. Tunnermann, "SPM-induced spectral compression of picosecond pulses in single-mode Yb-doped fiber amplifier," *Appl. Phys. B.*, vol. 74, no. 2, pp. 191–195, Feb. 2002.

[4] R. Paschotta, J. Nilsson, A. C. Tropper, and D. C. Hanna, "Ytterbium-doped fiber amplifiers," *IEEE J. Quantum Electron.*, vol. 33, no. 7, pp. 1049–1056, Jul. 1997.

[5] J. Limpert, T. Schreiber, T. Clausnitzer, K. Kollner, H. J. Fuchs, E. B. Kley, H. Zellmer, and A. Tunnermann, "High-power femtosecond Yb-doped fiber amplifier," *Opt. Exp.*, vol. 10, no. 14, pp. 628–638, Jul. 2002.

[6] V. I. Kruglov, A. C. Peacock, J. D. Harvey, and J. M. Dudley, "Self-similar propagation of parabolic pulses in normal-dispersion fiber amplifiers," *J. Opt. Soc. Amer. B.*, vol. 19, no. 3, pp. 461–469, Mar. 2002.

[7] A. C. Peacock, R. J. Kruhlak, J. D. Harvey, and J. M. Dudley, "Solitary pulse propagation in high gain optical fiber amplifiers with normal group velocity dispersion," *Opt. Commun.*, vol. 206, no. 1, pp. 171–177, May 2002.

[8] D. B. S. Soh, J. Nilsson, and A. B. Grudinin, "Efficient femtosecond pulse generation using a parabolic amplifier combined with a pulse compressor. II. Finite gain-bandwidth effect," *J. Opt. Soc. Amer. B.*, vol. 23, no. 1, pp. 10–19, Jan. 2006.

[9] J. Paye, "The chronocyclic representation of ultrashort light pulses," *IEEE J. Quantum Electron.*, vol. 28, no. 10, pp. 2262–2273, Oct. 1992.

[10] E. Yahel, O. Hess, and A. Hardy, "Spectrally resolved approach for modeling short pulse amplification in Er^{3+}-doped fibers," *IEEE Photon. Technol. Lett.*, vol. 18, no. 21, pp. 2227–2229, Nov. 2006.

[11] E. Yahel, O. Hess, and A. Hardy, "Analysis of nonlinear gain-induced effects on short pulse amplification in doped fibers by use of an extended power equation," *Opt. Lett.*, vol. 32, no. 2, pp. 118–120, Jan. 2007.

[12] A. W. Snyder and J. D. Love, *Optical Waveguide Theory*, 1st ed. New York: Chapman and Hall, 1973.

[13] E. Desurvire, "Study of the complex atomic susceptibility of erbium-doped fiber amplifiers," *J. Lightw. Technol.*, vol. 8, no. 10, pp. 1517–1527, Oct. 1990.

[14] E. Desurvire, *Erbium-Doped Fiber Amplifiers Principles and Applications*, 1st ed. New York: Wiley, 1994, ch. 4.

[15] M. Janos and S. C. Guy, "Signal-induced refractive index changes in erbium-doped fiber amplifiers," *J. Lightw. Technol.*, vol. 16, no. 4, pp. 542–548, Apr. 1998.

[16] J. W. Arkwright, P. Elango, G. R. Atkins, T. Whitbread, and M. J. F. Digonnet, "Experimental and theoretical analysis of the resonant nonlinearity in ytterbium-doped fiber," *J. Lightw. Technol.*, vol. 16, no. 5, pp. 798–806, May 1998.

[17] Y. R. Shen, *The Principles of Nonlinear Optics*. Hoboken, NJ: Wiley, 2003.

[18] E. G. Harris, "Radiative transfer in dispersive media," *Phys. Rev.*, vol. 138, no. 2B, pp. 479–485, Apr. 1965.

[19] G. C. Pomraning, "Radiative transfer in dispersive media," *Astrophys. J.*, vol. 153, pp. 321–324, Jul. 1968.

[20] G. C. Pomraning, *The Equations of Radiation Hydrodynamics*, 1st ed. Oxford, U.K.: Pergamon, 1973.

[21] G. P. Agrawal, *Nonlinear Fiber Optics*, 3rd ed. San Diego, CA: Academic, 2001.

[22] C. H. Henry, "Theory of spontaenous emission noise in open resonators and its application to lasers and optical amplifiers," *J. Lightw. Technol.*, vol. LT-4, no. 3, pp. 288–297, Mar. 1986.

[23] M. Hofer, M. E. Fermann, A. Galvanauskas, D. Harter, and R. S. Windeler, "Low-noise amplification of high-power pulses in multimode fibers," *IEEE Photon. Technol. Lett.*, vol. 11, no. 6, pp. 650–652, Jun. 1999.

[24] J. M. Dudley, L. P. Barry, P. G. Bollond, J. D. Harvey, and R. Leonhardt, "Characterizing pulse propagation in optical fibers around 1550 nm using frequency-resolved optical gating," *Opt. Fiber Technol.*, vol. 4, no. 3, pp. 237–265, Jul. 1998.

[25] Q. Chang, E. Jia, and W. Sun, "Difference schemes for solving the generalized nonlinear schroedinger equation," *J. Comput. Phys.*, vol. 148, pp. 397–415, Jan. 1999.

[26] L. Cohen, "Time-frequency distributions—A review," *Proc. IEEE*, vol. 77, no. 7, pp. 941–981, Jul. 1989.

[27] J. Nilsson, W. A. Clarkson, R. Selvas, J. K. Sahu, P. W. Turner, S. U. Alam, and A. B. Grudinin, "High-power wavelength-tunable cladding-pumped rare-earth-doped silica fiber lasers," *Opt. Fiber Technol.*, vol. 10, no. 1, pp. 5–30, Jan. 2004.

[28] D. B. S. Soh, J. Nilsson, and A. B. Grudinin, "Efficient femtosecond pulse generation using a parabolic amplifier combined with a pulse compressor. I. stimulated raman-scattering effects," *J. Opt. Soc. Amer. B.*, vol. 23, no. 1, pp. 1–9, Jan. 2006.
[29] A. Malinkowski, A. Piper, J. H. V. Price, K. Furusawa, Y. Jeong, J. Nilsson, and D. J. Richardson, "Ultrashort-pulse Yb^{3+}-fiber-based laser and amplifier system producing $>$25-W average power," *Opt. Lett.*, vol. 29, no. 17, pp. 2073–2075, Sep. 2004.
[30] J. Limpert, A. Liem, T. Gabler, H. Zellmer, A. Tunnermann, S. Unger, S. Jetschke, and H. R. Muller, "High-average-power picosecond Yb-doped fiber amplifier," *Opt. Lett.*, vol. 26, no. 23, pp. 1849–1851, Dec. 2001.

Eldad Yahel received the B.Sc. degree in physics and materials engineering from Ben-Gurion University of the Negev, Beer-Sheva, Israel, in 1998 and the M.Sc. degree in electrical engineering from Tel-Aviv University, Tel-Aviv, Israel, in 2002. He is currently working toward the Ph.D. degree at the Advanced Technology Institute, University of Surrey, Surrey, U.K.

From 1999 to 2002, he was with the Department of Electrical Engineering—Physical Electronics, Tel Aviv University, Israel, conducting research on $Er^{3+} - Yb^{3+}$ codoped fiber lasers and amplifiers.

Ortwin Hess received the B.Sc. degree in physics at the University of Erlangen, Erlangen, Germany, in 1987 and the M.Sc. and Ph.D. degrees at the Technical University of Berlin, Berlin, Germany, in 1990 and 1993, respectively. He holds a Habilitation in theoretical physics from the University of Stuttgart , Stuttgart, Germany (1997).

He is a Professor of computational quantum electronics and leads the Theory and Advanced Computation (TAC) Group at the Advanced Technology Institute, University of Surrey, Surrey, U.K. He has been visiting professor at Stanford University, Stanford, CA, and the University of Munich, Germany. His research interests are focused on the supercomputer simulation of the ultrafast spatiotemporal dynamics of semiconductor lasers and novel high-speed optoelectronic devices (quantum-dot and quantum-well lasers, high-power semiconductor optical amplifiers, and microcavities). His current interests encompass ultrafast effects in active semiconductor media, mesoscopic quantum electronics (quantum fluctuations, microcavity lasers, control of spontaneous emission, optical molecular motors, and biophotonics), photonic materials (quantum dots, photonic crystals, synthetic opals, liquid crystals, and biomolecules), as well as nanothermodynamics and nonlinear nanorheology.

Amos A. Hardy (SM'84–F'97) received the B.Sc. and M.Sc. degrees in physics from the Hebrew University of Jerusalem, Jerusalem, Israel, and the Ph.D. degree in applied physics from the Weizmann Institute of Science, Rehovot, Israel, in 1966, 1969, and 1975, respectively.

From 1975 to 1983, he was with the Department of Electronics, Weizmann Institute of Science. While at the Weizmann Institute, he held the Ruth E. Recu Career Development Chair. From 1976 to 1979, he was on leave at Stanford University, Stanford, CA, working on various laser resonator problems, optical phase conjugation, and optical rotation-sensing systems. During the summer of 1982, he was a Visiting Scientist at Bell Laboratories, Holmdel, NJ, where he worked on problems related to DFB lasers. Since 1983, he has been with the Faculty of Engineering, Tel-Aviv University, Tel Aviv, Israel, where he was appointed Associate Professor and later promoted to Professor in 1988. From 1991 to 1995, he served as Chairman of the Department of Electrical Engineering—Pysical Electronics. From June 1984 to July 1985, he was a Visiting Scientist at Xerox Palo Alto Research Center (PARC), Palo Alto, CA, where he was engaged in the analysis of phase-coupled laser arrays. During the summers of 1985 and 1986, he was a Visiting Associate Professor at the Center for High Technology Materials, University of New Mexico. He was on sabbatical leave as a Senior Research Scientist at Spectra Diode Laboratories (SDL) during the academic year of 1988–1989 and also spent several summers there. During these visits, he was engaged in the analysis of grating-coupled surface emitters, flared amplifiers, laser arrays, and fiber lasers and amplifiers. In 1994 and 1995, he spent several months as Visiting Professor at Ecole Polytechnique Federale de Lausanne (EPFL), Lausanne, Switzerland, where he was engaged in DFB and vertical-cavity lasers' theory. For several months in 1997, 1998, and 1999, he was a Visiting Scientist at Uniphase Laser Enterprise (formerly IBM Laboratories), Zurich, Switzerland, where he was engaged in problems related to ridge lasers.

Dr. Hardy serves on the Editorial Board for the *Journal of Microwave and Optical Technology Letters*. He received the "Polish Jewish Ex-Servicemen Association—London" prize in the field of Applied Electronics in 1993 for his contributions to the analysis and design of high-power coherent diode lasers. He is a Fellow of the Optical Society of America.